

Article

Mechanical Behavior of Al–Al₂Cu–Si and Al–Al₂Cu Eutectic Alloys

Qian Lei ^{1,2}, Jian Wang ^{3,*} and Amit Misra ^{1,*}

¹ Department of Materials Science and Engineering, College of Engineering, University of Michigan–Ann Arbor, Ann Arbor, MI 48109, USA; leiqian@csu.edu.cn

² State Key Laboratory for Powder Metallurgy, Central South University, Changsha 410083, China

³ Department of Mechanical and Materials Engineering, University of Nebraska–Lincoln, Lincoln, NE 68588, USA

* Correspondence: jianwang@unl.edu (J.W.); amitmis@umich.edu (A.M.)

Abstract: In this study, laser rapid solidification technique was used to refine the microstructure of ternary Al–Cu–Si and binary Al–Cu eutectic alloys to nanoscales. Micropillar compression testing was performed to measure the stress–strain response of the samples with characteristic microstructure in the melt pool regions. The laser-remelted Al–Al₂Cu–Si ternary alloy was observed to reach the compressive strength of 1.59 GPa before failure at a strain of 28.5%, which is significantly better than the as-cast alloy with a maximum strength of 0.48 GPa at a failure strain of 4.8%. The laser-remelted Al–Cu binary alloy was observed to reach the compressive strength of 2.07 GPa before failure at a strain of 26.5%, which is significantly better than the as-cast alloy with maximum strength of 0.74 GPa at a failure strain of 3.3%. The enhanced compressive strength and improved compressive plasticity were interpreted in terms of microstructural refinement and hierarchical eutectic morphology.

Keywords: rapid solidification; compression; micropillar



Citation: Lei, Q.; Wang, J.; Misra, A. Mechanical Behavior of Al–Al₂Cu–Si and Al–Al₂Cu Eutectic Alloys. *Crystals* **2021**, *11*, 194. <https://doi.org/10.3390/cryst11020194>

Academic Editor: Ronald W. Armstrong

Received: 23 January 2021

Accepted: 12 February 2021

Published: 16 February 2021

Publisher's Note: MDPI stays neutral with regard to jurisdictional claims in published maps and institutional affiliations.



Copyright: © 2021 by the authors. Licensee MDPI, Basel, Switzerland. This article is an open access article distributed under the terms and conditions of the Creative Commons Attribution (CC BY) license (<https://creativecommons.org/licenses/by/4.0/>).

1. Introduction

Metal-based eutectic composites exhibit periodic microstructures with lamellar, fibrous, degenerate, or other morphologies and are widely studied as model systems for understanding microstructure evolution under solidification conditions [1]. These microstructures typically contain intermetallic or other hard phases, which results in high hardness, suggesting potential for technological applications at ambient and elevated temperatures [2,3]. A limitation for all the as-cast metal–intermetallic eutectic systems has been the lack of plastic deformability [2,3], often even under compression loading. Recent work on a chill cast or laser surface-remelted eutectics has shown that high strength at room temperature can be achieved without loss of plastic deformability in a wide range of refined eutectic microstructures in Al–, Ti–, Ni–, Zn–, and Fe-based alloys [4–16].

In our earlier work, in situ micro-pillar compression testing in a scanning electron microscope (SEM) was used to characterize the stress–strain response of laser surface remelted Al–Al₂Cu eutectic alloys [15]. For micro-pillar compression from within a single eutectic colony, the plasticity mechanisms were observed to depend strongly on the orientation of the lamellae with respect to the loading direction. For compression axis 90° to the lamellae, the highest yield strength was observed with negligible global plasticity due to localized shear failure, whereas for compression axis close to 0° to the lamellae, buckling and kinking occurred. In the case of a loading axis near 45° to lamellae, sliding along Al–Al₂Cu lamellar interfaces was reported with the lowest yield strength [15]. Polycrystalline eutectics with the inter-lamellar spacing of ~20 nm exhibited a maximum flow strength of approximately 1.6 GPa and plasticity of approximately 17%. Bimodal morphologies in Al–Al₂Cu containing degenerate, wavy, morphology dispersed with nanoscale lamellar eutectic resulted in high plasticity that was uniformly distributed throughout the height of the compression

sample at a strength level of 1.36 GPa [15]. The role of the mixed and bimodal morphology in promoting high strength and plasticity was not clearly elucidated, particularly for binary vs. ternary systems.

In this work, laser surface remelting was used to refine the eutectic morphology of Al–Al₂Cu–Si eutectic and compared with binary Al–Al₂Cu, processed and tested with the same approach. A focused ion beam (FIB) was employed to fabricate cylindrical micro-pillars from laser-remelted alloys. Nano-indenter was used to compress the micropillars. The compression behaviors of the micropillars were investigated systematically; the cracking and co-deformation mechanism of the binary and ternary eutectics are discussed below.

2. Experimental Procedure

The Al–Al₂Cu–Si (Al₈₁Cu₁₃Si₆, at%) and Al–Al₂Cu (Al₈₁Cu₁₉, at%) eutectic as-cast ingots were fabricated by an arc-melter at the Materials Preparation Center, Ames Laboratory, Iowa State University, under a protective argon gas environment. Plates with dimensions of 20 × 10 × 2 mm³ were cut from the as-cast ingot. The plates were mechanically ground and polished. Laser surface processing experiments were conducted on a solid-state disk laser (TRUMPF Laser HLD 4002 (Trumpf Laser, Plymouth, MI, USA) at a wavelength of 1.03 μm. Details of synthesis and laser re-melting have also been published elsewhere [17,18]. In an earlier study [18], the effects of the processing parameters on the microstructures of Al–Cu–Si ternary eutectic were reported. The laser power was varied between 500 and 1000 W and the laser spot diameter and scan speed ranged from 0.8 to 1.2 mm and 2.54 to 101.4 mm/s, respectively. In this study, samples processed with nominal parameters of 500 W laser power, 2.54 mm/s scan speed, and 1 mm spot size were used for micropillar compression testing. Argon shielding gas (flow rate of 9.4 L/min) was used during the laser melting process to prevent oxidation. The micropillar compression tests were performed on a TI-750 TriboIndenter (Bruker, Minneapolis, MN, USA) with a conical indenter in displacement-control mode, and the experimental compressive strain rate was 2.5 × 10^{−2}·s^{−1}. An FEI Helios 650 NanoLab dual-beam scanning electron microscope (SEM) was used to capture the microstructures of the eutectic micropillars before and after compression tests. Thin foil samples fabricated by FIB were studied on a JEOL 3011 transmission electron microscope (TEM) with an operating voltage of 300 kV.

3. Experimental Results

Figure 1 shows the cross-section view of the laser-remelted molten and local regions in Al–Al₂Cu and Al–Al₂Cu–Si eutectics. As shown in Figure 1a, the as-cast Al–Al₂Cu eutectic structures can be divided into lamellae and degenerates, resulting from different heat transfer characteristics during solidification [9]. However, only lamellae Al–Al₂Cu eutectics can be observed in the laser-remelted sample (Figure 1b). In the backscattered electron (BSE) images (Figure 1a,b), the phases in the bright and dark contrasts are Al₂Cu and Al, respectively. The inter-lamellar spacing (λ) was statistically analyzed and was observed to decrease from 1400 ± 200 nm (as-cast) to 39 ± 4 nm (laser-treated region). The refined Al–Al₂Cu eutectics should be ascribed to the high heating and cooling rate of the laser surface processing technique [7,8,13]. In the Al–Al₂Cu–Si eutectics, Al (dark), Al₂Cu (bright), and Si (gray) were detected in the as-cast Al–Al₂Cu–Si samples (Figure 1c), while there were bimodal structures with dendrite structure of Al (dark) + Al₂Cu (bright) and lamellae structure (Al–Al₂Cu–Si) in the laser-remelted Al₂Cu–Si eutectics (Figure 1d).

Four Al–Al₂Cu–Si micropillars cut from the laser-treated (LT) region and as-cast base are named laser-remelted and as-cast lamellae, respectively. Three Al–Al₂Cu micropillars cut from the laser-treated (LT) region and as-cast base are labelled as-cast lamellae, as-cast degenerate, and laser-remelted lamellae. The applied compression force (F) and the immediate height (h_I) of the pillar were recorded. An average diameter (d) of the top, middle, and bottom of each pillar was employed to calculate the stress and the strain. The engineering stress (σ_E) was computed by dividing the applied force (F) by the average cross-section area (π × d × d/4), σ_E = F/(π × d × d/4). The engineering strain (ε_E) was obtained by dividing the height

variation of the pillar by the original height of the pillar (h_0), $\varepsilon_E = (h_1 - h_0)/h_0$. The engineering stress (σ_E) versus engineering strain (ε_E) curves of the Al–Al₂Cu–Si and Al–Al₂Cu eutectic micro-pillars are depicted in Figure 2, in which the as-cast Al–Al₂Cu + Si eutectics exhibit ultimate engineering stress of 480 MPa and a total strain to fracture of 4.8%, while the laser-treated Al–Al₂Cu + Si eutectics with bimodal structures exhibit both the highest ultimate engineering stress of 1586 MPa and the highest fracture strain of 28.5%. The as-cast Al–Al₂Cu lamellae and degenerate eutectics exhibit ultimate engineering stress of 742 MPa and 1180 MPa and total strains to fracture of 3.3% and 5.6% respectively. The laser-treated Al–Al₂Cu lamellae exhibit ultimate engineering stress of 2075 MPa and a total strain to fracture of 26.5%, as summarized in Table 1. This suggests that laser surface processing can effectively improve both the strength and plastic deformability of Al–Al₂Cu–Si and Al–Al₂Cu eutectics. The high strength of laser-treated Al–Al₂Cu lamellae eutectics should be ascribed to the nanoscale lamellar spacing. Decreasing the inter-lamellar spacing results in more Al–Al₂Cu phase boundaries (PB) being introduced, facilitates the dislocation–PB interactions, and affords more room for dislocation storage, which sustains more pronounced strain hardening in the Al–Al₂Cu eutectics [16,19].

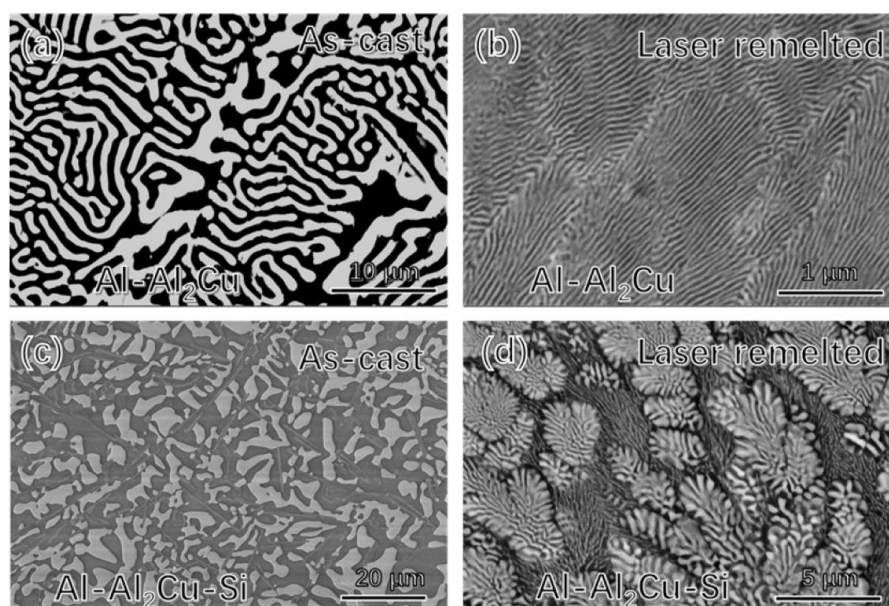


Figure 1. Backscattered electron (BSE) images of the microstructure of as-cast Al–Al₂Cu and Al–Al₂Cu–Si eutectics; (a) as-cast Al–Al₂Cu; (b) laser-remelted Al–Al₂Cu; (c) as-cast Al–Al₂Cu–Si; (d) laser-remelted Al–Al₂Cu–Si.

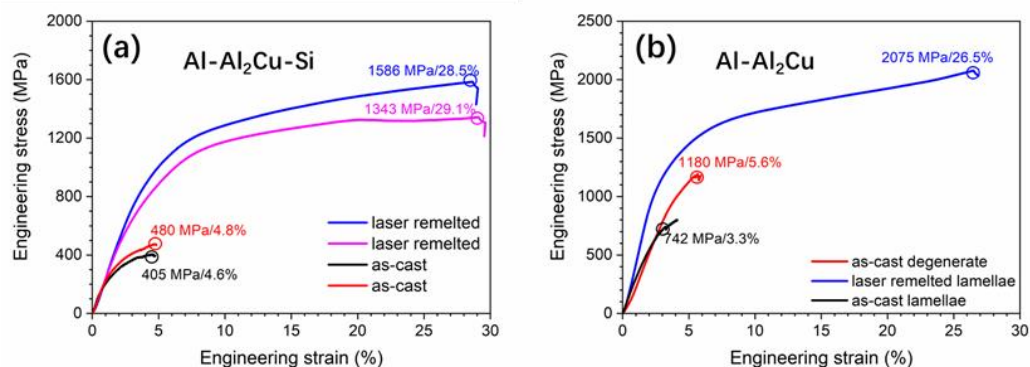


Figure 2. Compressive engineering stress—engineering strain curves of micropillars with different microstructures: (a) Al–Al₂Cu–Si eutectic; (b) Al–Al₂Cu eutectic. The strain to fracture and the maximum compress flow stress before fracture are presented.

Table 1. Microstructure and compressive properties of the studied eutectic alloys.

Eutectics	Processing	Morphology	Strain to Fracture (%)	Maximum Strength (MPa)
Al–Al ₂ Cu	As-cast	Lamellae	3.3	742
Al–Al ₂ Cu	As-cast	Degenerate	5.6	1180
Al–Al ₂ Cu	Laser-remelted	Lamellae	26.5	2075
Al–Al ₂ Cu–Si	As-cast	Mixed	4.8	480
Al–Al ₂ Cu–Si	As-cast	Mixed	4.6	405
Al–Al ₂ Cu–Si	Laser-remelted	Bimodal	29.1	1343
Al–Al ₂ Cu–Si	Laser-remelted	Bimodal	28.5	1586

Figure 3 shows the macro- and micro-structures of the Al–Al₂Cu–Si pillars before and after compression tests. Microstructures of the as-cast Al–Al₂Cu–Si eutectic micropillars before and after the compression test are shown in Figure 3a1,a2. Microstructures of the laser-treated Al–Al₂Cu–Si eutectic micropillars before and after the compression test are shown in Figure 3b,c. Micro-cracks were detected in the compressed as-cast Al–Al₂Cu–Si eutectic micropillars (Figure 3a2–a4). The detected micro-cracks on the Si and Al₂Cu phases indicated that the stress concentration occurred on the boundaries between Si and the other as-cast eutectics, while there were no micro-cracks detected in the laser-treated Al–Al₂Cu+Si eutectic micropillars (Figure 3b2–c4). The laser-treated Al–Al₂Cu–Si eutectics presented good deformation capability.

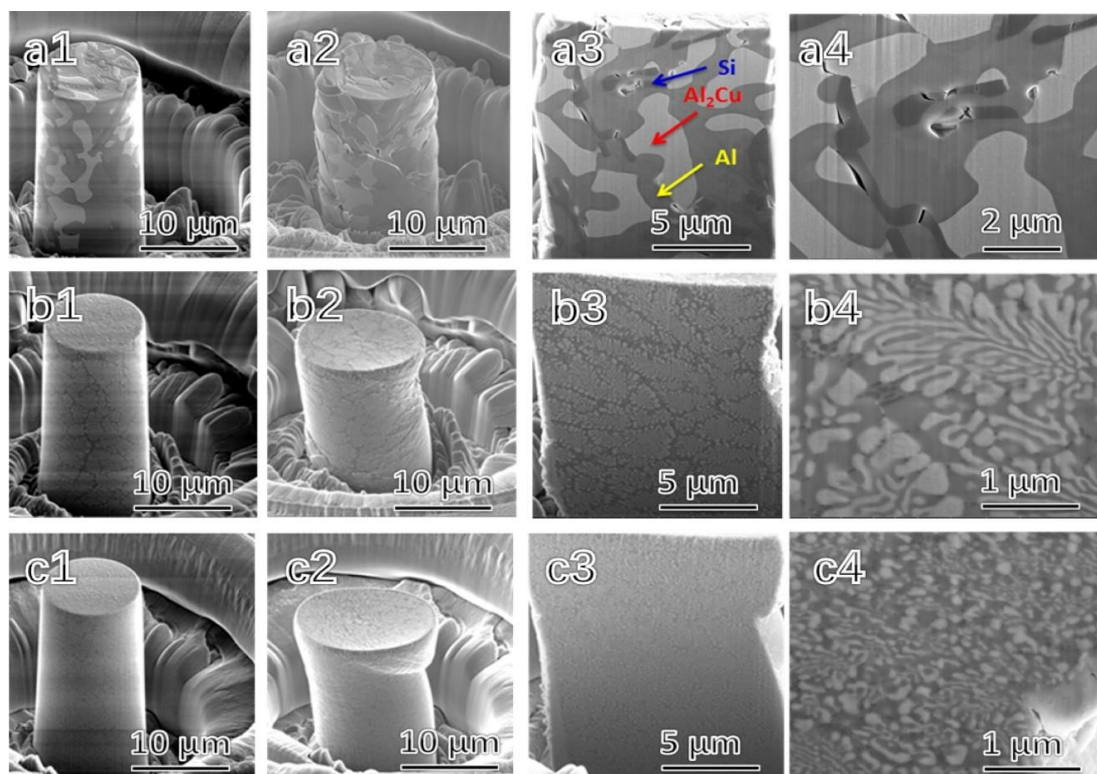


Figure 3. Macro- and micro-structures of the Al–Al₂Cu–Si pillars before and after compression test; (a1–c1) the as-cast, laser treated, refined laser remelted pillars before compression; (a2–c2) the pillars after compression; (a3–c3) the cross-section of the pillars after compression; (a4–c4) the high magnification images of the images from a3–c3. All the images were captured in the SEM with a tilt angle of 52°.

Figure 4 shows the macro- and micro-structures of the Al–Al₂Cu pillars before and after compression tests. The phases in the bright and dark contrasts are Al₂Cu and Al in the BSE images (Figure 4) and TEM image (Figure 4c3). Before compressive tests, the size

and shape of these micro-pillars are nearly identical. Both lamellae and degenerate as-cast eutectics show the distinct interface of α -Al and θ -Al₂Cu phases (Figure 4a1,b1); however, the interface cannot be distinguished clearly for the laser-treated lamellae eutectics because of their nanoscale inter-lamellar spacing (Figure 4c1). The microstructures of the as-cast Al–Al₂Cu lamellar eutectics micropillars before and after the compression tests are shown in Figure 4a1,a2, and Figure 4a3 is the section view of the compressed pillar. Micro-cracks were detected on the Al₂Cu lamellae inside the compressed micropillar (Figure 4a2,a3), and two voids were formed inside the Al₂Cu (Figure 4a3). The microstructures of the laser-treated Al–Al₂Cu+Si degenerate eutectics micropillars before and after the compression tests are shown in Figure 4b1,b2. Micro-cracks were also detected on the Al₂Cu lamellae. The microstructures of the laser-treated Al–Al₂Cu+Si eutectics micropillars before and after the compression test are shown in Figure 4c1,c2. There were no micro-cracks detected in the laser-treated Al–Al₂Cu eutectics micropillars (Figure 4c2). Further TEM characterization in Figure 4c3 revealed that cracking in θ -Al₂Cu phase was suppressed in the laser-treated nanoscale Al–Al₂Cu eutectics; α -Al and θ -Al₂Cu phases were observed to co-deform together with some distinct dislocation transmission across Al–Al₂Cu interfaces, as pointed out by red arrows. After compressive tests, apparent cracks could be observed in θ -Al₂Cu layers for as-cast lamellae eutectics with 3.22% reduction and as-cast degenerate eutectics with 4.69% reduction. A similar phenomenon was observed in our previous works, in which after indentation tests, Al–Al₂Cu eutectics with microscale inter-lamellar spacing exhibited cracking in the θ -Al₂Cu phase, owing to their brittle nature at room temperature [2,3]. The angles of the crack propagation direction were detected to be 48.5° and 47.7° tilted along the loading direction for as-cast lamellae and as-cast degenerated, respectively (Figure 4a2,b2). However, no crack was detected in the laser-treated lamellae eutectics with a 10.36% reduction. The microstructure of the compressed micropillars indicated that the laser-treated Al–Al₂Cu eutectics present much higher deformation capability than the as-cast Al–Al₂Cu eutectics. The high strength of laser-treated lamellae should be ascribed to the nanoscale lamellar spacing. Decreasing the inter-lamellar spacing results in more Al–Al₂Cu phase boundaries (PB) being introduced, facilitates the dislocation-PB interactions, and affords more room for dislocation storage, which sustains more pronounced strain hardening in the Al–Al₂Cu eutectics [19].

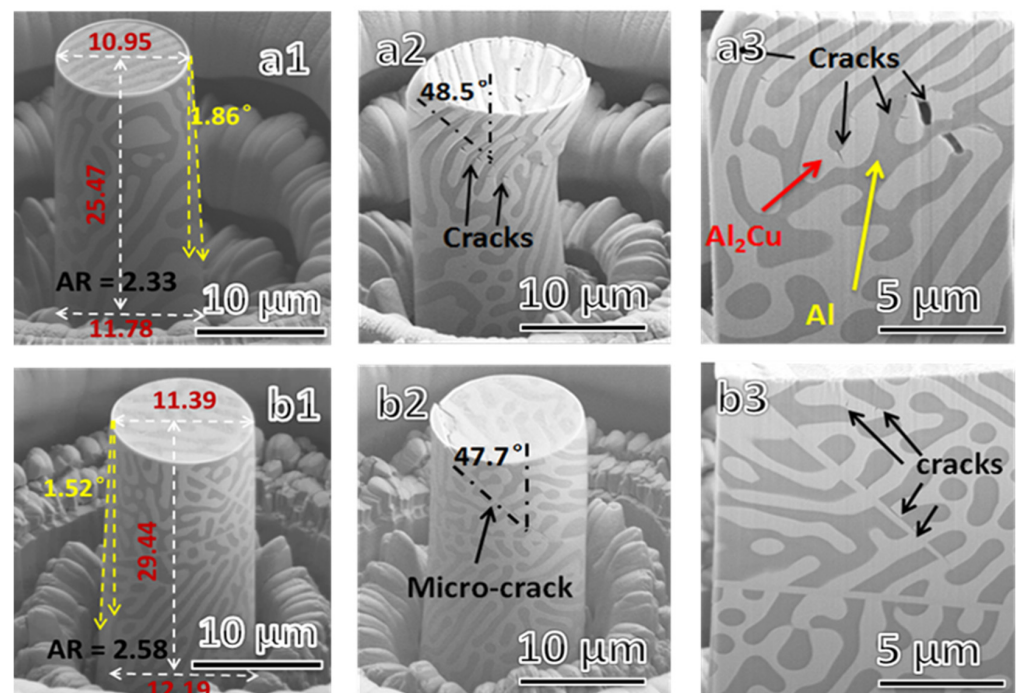


Figure 4. Cont.

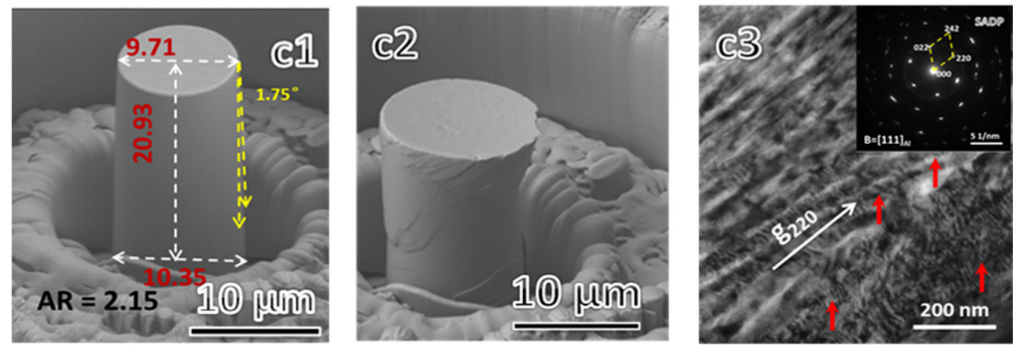


Figure 4. Macro- and micro-structures of micropillars before and after compressive tests from the Al–Al₂Cu eutectics with different structures of (a) as-cast lamellae, (b) as-cast degenerate, and (c) laser-remelted lamellae; (a1–c1) the micropillars before compression; (a2–c2) the micropillars after compression; (a3,b3) the cross-section views; (c3) the TEM image of the cross-section view. All images except c3 were captured in the SEM with a tilt angle of 52°.

4. Discussion

4.1. Strengthening Mechanisms

To further understand the strengthening mechanism of the laser-treated Al–Al₂Cu–Si and Al–Al₂Cu eutectics, it is essential to consider the roles of interfaces (soft Al phase and hard Al₂Cu or Si phase) when the interspacing is refined to nanometer size. In this case, the empirical rule of the mixture is invalid. In this work, the volume fractions of each phase in the studied eutectics are the same even though the length scale has been changed.

A classical constitutive model of the composite structure containing the soft phase and the hard phase could be written as follows:

$$\sigma_m = E_m \cdot \varepsilon_m, \sigma_m < \sigma_m^{\text{yield}} \quad (1)$$

$$\sigma_m = E_m \cdot \varepsilon_m + K_m \cdot \varepsilon_m, \sigma_m > \sigma_m^{\text{yield}} \quad (2)$$

where the subscript (m) infers to either soft phase (s) or hard phase (h). Here, the uniform stress at the ends of the hard phase, and the soft phase is unaltered with the displacement. It is important to convert the stress and strain into a more fundamental quantity (e.g., energy density). For individual phase, the total work density can be expressed by integrating the area under the stress-strain curve as follows:

$$W_m = \frac{1}{2} \frac{(\sigma_m^{\text{yield}})^2}{E_m} + \sigma_m^{\text{yield}} \cdot \left(\frac{\sigma_m^{\text{yield}}}{E_m} - \varepsilon_{\text{max}} \right) + \int_{\frac{\sigma_m^{\text{yield}}}{E_m}}^{\varepsilon_{\text{max}}} [K_m (\varepsilon_m)^{n_m}] - \sigma_i^{\text{yield}}] \cdot d\varepsilon - \frac{1}{2} \frac{P_{\text{max}}}{A} (\varepsilon_{\text{max}} - \varepsilon_{pi}) \quad (3)$$

where the subscript (m) infers to either the soft phase (s) or the hard phases (h). ε_p , ε_{max} , and P_{max} are the plastic parts of the true-strain and maximum true-strain induced in the experiment and the corresponding maximum indentation load, respectively. We hypothesize that the energies of interaction at the lamellar interfaces (soft Al and hard Al₂Cu or Si) play significant roles in the tensile test's deformation process. The total work density of the composites (\bar{W}) can be divided into a plastic part and an elastic part, with respective interfacial energy terms (denoted by superscript “interface”), as follows:

$$\bar{W} = [W_e^h + W_e^s + W_e^{\text{interface}}] + [W_p^h + W_p^s + W_p^{\text{interface}}] \quad (4)$$

The elastic part of the energy of the effective composite equates to the total elastic energy, since there is no other phase combination, therefore a corresponding equation can be written as follows:

$$\frac{1}{2} \cdot \bar{E} \cdot \varepsilon^2 (h_s + h_h) = \frac{1}{2} E_m \varepsilon^2 h_s + \frac{1}{2} E_f \varepsilon^2 h_h + W_e^{\text{interface}}, \quad \varepsilon \ll \frac{\sigma_i^{\text{yield}}}{E_i} \quad (5)$$

where h_s is the thickness of the soft phase (Al) and h_h is the thickness of the hard phase (Al₂Cu or Si), and $W_e^{\text{interface}}$ is the elastic energy contribution of the interface. The inter-lamellar spacing, $\lambda=(h_1+h_2)/2$, becomes the function of the lamellar geometry. The plastic part of the energy of the composite can be equated with total plastic energy due to the pure phase combination, therefore a corresponding equation can be written as follows:

$$\left[\bar{\sigma}^{\text{yield}} \varepsilon_e + \int_{\varepsilon_e}^{\varepsilon} \bar{K} \varepsilon^n d\varepsilon \right] (h_1 + h_2) \cong \left[\bar{\sigma}_m^{\text{yield}} \varepsilon_e^m + \int_{\varepsilon_e}^{\varepsilon} \bar{K}_m (\varepsilon_m)^{n^m} d\varepsilon \right] h_1 + \left[\bar{\sigma}_f^{\text{yield}} \varepsilon_e^f + \int_{\varepsilon_e}^{\varepsilon} \bar{K}_f (\varepsilon_f)^{n^f} d\varepsilon \right] h_2 + W_P^{\text{interface}} \quad (6)$$

Combining the above two energy equations as described in Equation (4), a total energy balance is obtained. This allows us to evaluate the effect of the length scale of microstructure as expressed through k on the mechanical properties. Therefore, with the knowledge of inter-lamellar spacing k and the properties of the composite and pure phase, one can estimate the contribution of the interface to the overall elastic energy balance.

In order to verify the above relationships, the Al–Al₂Cu+Si eutectic was selected as an example. This eutectic comprises alternate plates of soft phase (Al) and hard phase (Al₂Cu and Si) intermetallic phases due to the variation in the lamellar spacing with the cooling rate. The mechanical properties of localized regions were further evaluated from a load-displacement curve obtained by the use of micropillar compression technique. The measured true-stress versus true-strain curves are shown in Figure 2.

4.2. Fracture Mechanisms

Eutectic alloys often exhibit poor fracture strength, which hinders their structural applications [9]. Recent studies have revealed significant improvements in fracture strength due to refinements of the microstructure [10–12]. Laser surface processing is an effective way to refine the microstructure, and it leads to a reduction in interlamellar spacing; it is evidence that microstructure refinement improves the plastic or fracture strain. These findings can be explained by two kinds of theoretical methods: one is a dislocation pile-up-based approach, and the other is a fracture-based approach. According to the dislocation-based approach, the deformation of eutectics is controlled by dislocation pile-ups at the interphase boundaries [20–22]. The interface between the soft phase (Al) and hard phase (Al₂Cu or Si) provides an obstacle for dislocation pile-up, which controlled the plasticity in this model. The interface hardening controls the yield strength. The stress arises irrespective of the detailed mechanism of the slip, since the plasticity is highly localized in such cases; here, the stress at the tip of the pile-up is given by [2].

$$\tau_p = \frac{K \cdot D \cdot \varepsilon_p}{b \cdot \sqrt{2\lambda}} \quad (7)$$

where K is the constant, D is the distance between the two dislocations, b is the Burger vector ($b = 0.285$ nm), λ is the lamellar spacing, and ε_p is the strain. Equation (6) indicates that the shear stress increases at a given strain with the decrease of inter-lamellar spacing, resulting in improvements in the strength of the eutectic alloy. This agrees well with the experimental data in this work.

Fracture is thought to be controlled by dislocation and interface behavior [23]. Griffith relation was applied in the other model based on crack propagation [3]. The critical crack size for cleavage crack propagation can be calculated as follows:

$$\sigma_F = \left[\frac{4 \cdot E \cdot \gamma}{\pi \cdot a \cdot (1 - \nu^2)} \right]^{0.5} \quad (8)$$

where σ_F is the fracture stress, E is the Young's modulus, γ is the surface energy (219.5 mJ/m² [24]), a is the critical crack length, and ν is the Poisson's ratio ($\nu_{\text{Al}} = 0.35$ and $\nu_{\text{Al}_2\text{Cu}} = 0.34$). Here, the Al–Al₂Cu eutectic is taken as an example for the analysis of the fracture mechanism. The Al₂Cu has a higher modulus (103 GPa) compared to Al (69 GPa). Substituting the above value, the fracture stress could be calculated: for Al

lamellar, $\sigma_F^{\text{Al}} = 101.34a^{-1/2}$, while for Al_2Cu , $\sigma_F^{\text{Al}_2\text{Cu}} = 180.415a^{-1/2}$. Thus, the fracture stress of Al_2Cu lamellar is larger than Al lamellar. As the eutectic micropillars were compressed, both Al lamellar and Al_2Cu lamellar were compressed, leading to plastic deformation. Since plastic deformation in Al lamella is easier than that in Al_2Cu lamella, the load transfers to Al_2Cu lamella; correspondingly, cracks were observed in Al_2Cu lamella (Figure 4a2,a3). For bulk materials, the critical crack length is mostly around a few millimeters to tens of millimeters, while the eutectic microstructure had two kinds of different ductility phases, whose critical crack length was limited by the inter-lamellar spacing. Supporting that the critical crack length is equal to the inter-lamellar spacing, the fracture stress increased dramatically as the inter-lamellar spacing was reduced from microscale to nanoscale. Thus, the laser-treated Al– Al_2Cu –Si and Al– Al_2Cu eutectics exhibit higher fracture strength and higher total strain to failure.

In summary, laser surface processing was conducted on Al– Al_2Cu –Si and Al– Al_2Cu eutectics to refine and manipulate the microstructures. Both laser-remelted ternary Al– Al_2Cu –Si and binary Al– Al_2Cu eutectics showed high strengths with maximum compressive strength of 1586 MPa and 2075 MPa and improved compressive plasticity with a failure strain of around 26%. By comparison, the as-cast ternary and binary eutectics with coarse microstructures exhibited low strength (lower than 740 MPa) and poor compressive plasticity (failure strain less than 5%). The enhanced compressive strength and improved compressive plasticity were interpreted in terms of microstructural refinement and hierarchical eutectic morphology. Laser-processed nanoscale eutectics show a bright promise of achieving ultra-high strength without loss of plastic deformability.

Author Contributions: Writing—original draft, Q.L.; Writing—review & editing, J.W. and A.M. All authors have read and agreed to the published version of the manuscript.

Funding: This research was funded by U.S. Department of Energy: DE-SC0016808.

Institutional Review Board Statement: Not applicable.

Informed Consent Statement: Not applicable.

Data Availability Statement: Not applicable.

Acknowledgments: This research was sponsored by DOE, Office of Science, Office of Basic Energy Sciences, grant DE-SC0016808. The authors acknowledge the assistance of J. Mazumder, B.P. Prashanth, and Y.C. Wang at the University of Michigan in material synthesis and laser surface treatment. Nanomechanical testing and electron microscopy were performed at the Michigan Center for Materials Characterization at the University of Michigan.

Conflicts of Interest: The authors declare no conflict of interest.

References

- Chanda, B.; Potnis, G.; Jana, P.P.; Das, J. A review on nano-/ultrafine advanced eutectic alloys. *J. Alloy. Compd.* **2020**, *827*, 154226. [[CrossRef](#)]
- Cantor, B.; Chadwick, G.A. The tensile deformation of unidirectionally solidified Al– Al_3Ni and Al– Al_2Cu eutectics. *J. Mater. Sci.* **1975**, *10*, 578–588. [[CrossRef](#)]
- Cantor, B.; May, G.J.; Chadwick, G.A. The tensile fracture behavior of the aligned Al– Al_3Ni and Al– CuAl_2 eutectics at various temperatures. *J. Mater. Sci.* **1973**, *8*, 830–838. [[CrossRef](#)]
- Park, J.M.; Mattern, N.; Kühn, U.; Eckert, J.; Kim, K.B.; Kim, W.T.; Chattopadhyay, K.; Kim, D.H. High-strength bulk Al-based bimodal ultrafine eutectic composite with enhanced plasticity. *J. Mater. Res.* **2009**, *24*, 2605–2609. [[CrossRef](#)]
- Han, J.H.; Kim, K.B.; Yi, S.; Park, J.M.; Sohn, S.W.; Kim, T.E.; Kim, D.H.; Das, J.; Eckert, J. Formation of a bimodal eutectic structure in Ti–Fe–Sn alloys with enhanced plasticity. *Appl. Phys. Lett.* **2008**, *93*, 141901. [[CrossRef](#)]
- Park, J.M.; Kim, T.E.; Sohn, S.W.; Kim, D.H.; Kim, K.B.; Kim, W.T.; Eckert, J. High strength Ni–Zr binary ultrafine eutectic-dendrite composite with large plastic deformability. *Appl. Phys. Lett.* **2008**, *93*, 031913. [[CrossRef](#)]
- Wang, Z.; Lin, X.; Cao, Y.; Huang, W. Microstructure evolution in laser surface remelting of Ni–33 wt.%Sn alloy. *J. Alloy. Compd.* **2013**, *577*, 309–314. [[CrossRef](#)]
- Wang, Z.; Zhang, Q.; Guo, P.; Gao, X.; Yang, L.; Song, Z. Effects of laser surface remelting on microstructure and properties of biodegradable Zn–Zr alloy. *Mater. Lett.* **2018**, *226*, 52–54. [[CrossRef](#)]

9. Park, J.; Kim, K.; Kim, D.; Mattern, N.; Li, R.; Liu, G.; Eckert, J. Multi-phase Al-based ultrafine composite with multi-scale microstructure. *Intermetallics* **2010**, *18*, 1829–1833. [[CrossRef](#)]
10. Park, J.M.; Kim, D.H.; Kim, K.B.; Eckert, J.M. Improving the plasticity of a high strength Fe–Si–Ti ultrafine composite by introduction of an immiscible element. *Appl. Phys. Lett.* **2010**, *97*, 251915. [[CrossRef](#)]
11. Tiwari, C.S.; Roy Mahapatra, D.; Chattopadhyay, K. *Appl. Phys. Lett.* **2012**, *101*, 171901. [[CrossRef](#)]
12. Zhang, L.; Lu, H.-B.; Mickel, C.; Eckert, J. Ductile ultrafine-grained Ti-based alloys with high yield strength. *Appl. Phys. Lett.* **2007**, *91*, 51906. [[CrossRef](#)]
13. Gouveia, G.L.; Kakitani, R.; Gomes, L.F.; Afonso, C.R.M.; Cheung, N.; Spinelli, J.E. Slow and rapid cooling of Al–Cu–Si ultrafine eutectic composites: Interplay of cooling rate and microstructure in mechanical properties. *J. Mater. Res.* **2019**, *34*, 1381–1384. [[CrossRef](#)]
14. Kim, J.T.; Lee, S.W.; Hong, S.H.; Park, H.J.; Park, J.Y.; Lee, N.; Seo, Y.; Wang, W.M.; Park, J.M.; Kim, K.B. Understanding the relationship between microstructure and mechanical properties of Al–Cu–Si ultrafine eutectic composites. *Mater. Des.* **2016**, *92*, 1038–1045. [[CrossRef](#)]
15. Wang, S.; Xie, D.; Wang, J.; Misra, A. Deformation behavior of nanoscale Al–Al₂Cu eutectics studied by in situ micropillar compression. *Mater. Sci. Eng. A* **2021**, *800*, 140311. [[CrossRef](#)]
16. Lien, H.-H.; Mazumder, J.; Wang, J.; Misra, A. Ultrahigh strength and plasticity in laser rapid solidified Al–Si nanoscale eutectics. *Mater. Res. Lett.* **2020**, *8*, 291–298. [[CrossRef](#)]
17. Lei, Q.; Ramakrishnan, B.P.; Wang, S.; Wang, Y.; Mazumder, J.; Misra, A. Structural refinement and nanomechanical response of laser remelted Al–Al₂Cu lamellar eutectic. *Mater. Sci. Eng. A* **2017**, *706*, 115–125. [[CrossRef](#)]
18. Ramakrishnan, B.P.; Lei, Q.; Misra, A.; Mazumder, J. Effect of laser surface remelting on the microstructure and properties of Al–Al₂Cu–Si ternary eutectic alloy. *Sci. Rep.* **2017**, *7*, 13468. [[CrossRef](#)]
19. Wang, S.; Liu, G.; Xie, D.; Lei, Q.; Ramakrishnan, B.; Mazumder, J.; Wang, J.; Misra, A. Plasticity of laser-processed nanoscale Al Al₂Cu eutectic alloy. *Acta Mater.* **2018**, *156*, 52–63. [[CrossRef](#)]
20. Liu, G.; Xie, D.; Wang, S.; Misra, A.; Wang, J. Mesoscale crystal plasticity modeling of nanoscale Al–Al₂Cu eutectic alloy. *Int. J. Plast.* **2019**, *121*, 134–152. [[CrossRef](#)]
21. Wang, J.; Misra, A. Strain hardening in nanolayered thin films. *Curr. Opin. Solid State Mater. Sci.* **2014**, *18*, 19–28. [[CrossRef](#)]
22. Armstrong, R.W. Size effects on material yield strength/deformation/fracturing properties. *J. Mater. Res.* **2019**, *34*, 2161–2176. [[CrossRef](#)]
23. Porter, D.; Easterling, K.; Smith, G. Dynamic studies of the tensile deformation and fracture of pearlite. *Acta Met.* **1978**, *26*, 1405–1422. [[CrossRef](#)]
24. Lewandowski, J.; Thompson, A. Micromechanisms of cleavage fracture in fully pearlitic microstructures. *Acta Metall.* **1987**, *35*, 1453–1462. [[CrossRef](#)]